Catal Lett (2007) 119:79–86
DOI 10.1007/s10562-007-9195-5

NO Reduction with CO on Copper and Ceria Oxides Supported on Alumina

M. Khristova · B. Ivanov · I. Spassova · T. Spassov

Received: 21 April 2007 / Accepted: 1 July 2007 / Published online: 19 August 2007

Keywords Alumina · Copper oxide · Ceria-based catalysts · NO reduction with CO · Transient response method · TPD

1 Introduction

The problem about decreasing the harmful emissions of nitrogen oxides in industrial gases or in motor vehicles is an important contemporary task in relation to the environmental protection and people health. Recently, the investigations on this topic increase because of the growing concern about ecological standards. One of the ways of neutralizing nitrogen oxides proposed by modern chemistry is their catalytic conversion to nitrogen.

Transition metal oxides have shown very good achievements with respect to NO reduction with CO [1]. The use of spinel catalysts, which are not sensitive to catalytic poisons, is also very helpful. In addition, the spinel formation affects favorably the reduction of oxides. The $Cu_xCo_{(3-x)}O_4$ spinel catalysts and those promoted with noble metals Pt-Rh/$CuCo_2O_4$/γ-Al_2O_3 are found to possess a high activity toward NO reduction with CO [2–6].

Jiang et al. [7] have established TiO_2- supported and CuO- promoted cerium to demonstrate a high activity in the NO + CO reaction, 100% conversion of NO being achieved at 300 °C. The high activity has been ascribed to the presence of four sites of NO adsorption NO (Cu^+, Cu^{2+}(I), Cu^{2+}(II) и Ce^{3+}) and Cu^{2+}(I)–Cu^+ и Ce^{3+}–Ce^{4+} containing active sites for the NO + CO reaction.

Studying the same reaction on preliminary reduced or re-oxidized CuO/TiO_2, Jiang et al. [8] observed an activity rising during the reduction of the catalyst surface. This was attributed to reduction-provoked appearance of "oxygen caves" on the catalyst surface, increasing Cu species dispersion and Cu(II) formation.

Park et al. [9] investigated the same catalyst type applied on Al_2O_3 and found the promotion of a cerium catalyst with copper to lead to an enhanced activity towards CO oxidation, the effect on methane oxidation being weaker.

Larsson et al. [10] have established that the modification of alumina support with ceria before the copper oxide deposition gives well dispersed copper oxide species and enhances the activity towards CO oxidation.

Zou et al. [11] has determined that the interfacial CuO and CeO_2 interaction and synergistic effect enhances the red–ox properties of CuO/CeO_2 catalyst and the highly dispersed copper species have been proposed as active sites for the selective CO oxidation.

The purpose of the present work is to investigate how the way and the sequence of copper and cerium oxide deposition on alumina influence on the activity of the prepared catalysts in the reduction of NO with CO.

2 Experimental

2.1 Catalyst Preparation

Three series of catalyst samples were prepared. Samples in which the active phase consisted of copper or cerium alone were also prepared for the sake of comparison. A 0.3—0.8 mm fraction of AlO(OH) Rhône Poulenc (AL) was

M. Khristova · B. Ivanov · I. Spassova (✉)
Institute of General and Inorganic Chemistry,
Bulgarian Academy of Sciences, Sofia 1113, Bulgaria
e-mail: ispasova@igic.bas.bg

T. Spassov
Faculty of Chemistry, University of Sofia, Sofia 1126, Bulgaria

used as a support. For the first series of samples, the support was at first impregnated with a copper solution, this being followed by impregnation with a cerium solution after calcination. For the second series of samples, the support was at first impregnated with a cerium solution, this being followed by impregnation with a copper solution after calcination. For the third series of samples, the two procedures were united, i.e. both metals were present in the impregnating solution. The impregnation took place in 16 h, after this the samples were dried for 2 h at 120 °C and calcined for 6 h at 350 °C. The impregnation was performed with nitrate metal solutions- $Cu(NO_3)_2$ and $(NH_4)_2Ce(NO_3)_6$ with concentrations of 8 g Cu for 100 mL water and 3.6 g Ce for 100 mL water. The ratio between the solution and the support volumes was 5:1. In this way, the following samples were obtained:

AlCuCe—prepared by successive impregnation of AL in the sequence impregnation with copper containing solution → calcinations → impregnation with cerium containing solution → calcination;
AlCeCu—prepared by successive impregnation of AL– in the sequence impregnation with cerium containing solution → calcination → impregnation with copper containing solution → calcination;
AlsCuCe—obtained by simultaneous impregnation of Al with a both metals in the impregnating solutions → calcination;
AlCu—prepared by impregnating AL with a solution containing copper alone → calcination;
AlCe—a product of the impregnation of AL with a solution of cerium only → calcination.

2.2 Catalyst Characterization

The Cu and Ce concentrations in the impregnation solution were determined by chemical analysis. The Cu and Ce content in the impregnated samples after extraction with HCl was determined by means atomic absorption spectroscopy (AAS) on a SP 191 device, manufactured by "Pye Unicam" Co.

X-ray diffraction (XRD) data were obtained using a Bruker D8 Advance diffractometer with Cu-Kα radiation and SolX detector.

The XPS measurements were done in the UHV chamber of ESCALAB-Mk II (VG Scientific) electron spectrometer with a base pressure of 1.10^{-8} Pa. The photoelectron spectra were excited using un-monochromatized Al $K\alpha_{1,2}$ radiation ($h\nu$ = 1486.6 eV). The binding energies (BE) were determined with an accuracy of ±0.1 eV utilizing the C1s line at 284.9 eV (from an adventitious carbon) as a reference. The composition and chemical surrounding of samples were investigated on the basis of the areas and binding energies of C1s, O1s, $Cu2p_{3/2}$, Ce3d, Al2p photoelectron peaks (after linear subtraction of the background) and Scofield's [12] photoionization cross-sections.

SEM studies were carried out on a JSM–5510 JEOL scanning electron microscope.

The texture characteristics were determined by low-temperature (77.4 K) nitrogen adsorption in a conventional volume apparatus. The specific surface area was calculated by the BET method. The total pore volume (V_t) was determined at a relative pressure $p/p_o = 0.95$.

2.3 Catalytic Activity Measurements

The catalytic experiments were carried out in a flow apparatus described in [2]. NO reduction with CO was investigated in the temperature range 25–300 °C. The catalytic tests were performed with a NO + CO + Ar gas mixture, containing 1200 ppm NO and 1200 ppm CO. Argon was used as a carrier gas at a total gas-flow rate of 433 $cm^3\ min^{-1}$ (space velocity 26,000 h^{-1}). A 1 cm^3 sample of a catalyst (the 0.3–0.8 mm fraction) was placed into the reactor with a quartz tube, d = 10 mm. After a catalytic test at 25 °C and isothermal desorption stage in Ar flow, temperature programmed desorption (TPD) was carried out in the same catalytic apparatus at a heating rate of 13 °C min^{-1} with an Ar flow in a range of 25–300 °C. The concentrations of NO and CO were continuously measured by gas analyzers. The outlet concentrations of NO and CO were controlled by a "UNOR 5 -Maihak" (Germany) and the CO_2 by an "Infralyt 2106" (Germany). The data were collected by a CSY-10 personal data station. Specord 75 IR (Germany) spectrophotometer with a 1 m folded path gas cell (Specac) were used for determination of the outlet N_2O content. The N_2 concentration in the outlet gas was determined on the basis of the material balance with respect to NO consumption.

Before a catalytic test, the catalysts were treated in an Ar flow at 300 °C for 1 h. Afterwards the reactor temperature was decreased to room temperature. The catalytic tests were performed with a gas mixture so that a red–ox index $[CO]_{inlet}/[NO]_{inlet} = 1 \pm 0.05$ was maintained, i.e. conditions close to the stoichiometric one are used. The chronology of this set of experiments involves a reaction stage (NO + CO + Ar flow) and an isothermal desorption stage (Ar flow) carried out at successively higher temperatures in the range from 50 to 300 °C. Each reaction stage lasts 30–35 min. After this time, the NO + CO + Ar flow is switched to Ar flow to perform an isothermal desorption stage (lasting 10 min). After that the temperature is set to the next desired value. The transient response method was

used to study the interaction of the gas phase with the catalyst surface. The method is based on the analysis of the response curves of the reaction products and allows determining the rate-controlling step of the catalytic reactions [13]. Kobayshi used this approach to analyze series model reactions and proposed a classification of the types of the response curves in dependence on the rate controlling stage of the catalytic process. This approach is successfully applied for the study of various reactions as well as the reduction of NO with CO.

3 Results and Discussion

3.1 Chemical Analysis and Adsorption Characteristics

Table 1 shows the chemical analysis results of the catalysts obtained, the impregnation solution concentrations, the BET specific surface areas and the phase composition determined by XRD.

Irrespectively to the fact that the impregnating solutions are with same Cu and Ce concentrations the samples contain different mass. % copper and cerium depending on the way of preparation. Hence, the method of preparation leads to the formation of different surface groups on the support. The XRD data of the support used indicate the presence of orthorhombic AlO(OH) only. All diffraction peaks are relatively broad, which evidences the fine crystalline nature of the support. With deposition of Ce alone, there are lines of CeO_2, those of the support being negligible in intensity. When Cu only is deposited, there are pronounced CuO peaks while those of the support are strongly suppressed and track of $CuAl_2O_4$ have been observed.

Well resolved peaks of CeO_2 are observed for AlsCuCe and AlCuCe, where track of $CuAl_2O_4$ are marked, while lines indicating copper oxide are not detected in the XRD patterns. Similar observations on Cu–Ce–O samples which do not show CuO reflection peaks have been reported by [13, 14]. The diffraction patterns of the AlCeCu contain mainly peaks for CeO_2 and CuO, $CuAl_2O_4$ being not observed. The study of the AlCeCu, AlsCuCe and AlCuCe with conventional XRD reveals that CeO_2 does not form a solid solution with CuO. The CuO is believed to precipitate probably throughout the grain boundaries of CeO_2. In contrast to the diffraction peaks of CuO, the ones of CeO_x are quite broadened and there the mean size found for the CeO_x crystallites is 10–15 nm. In the case of AlCeCu when the cerium is deposited first it hinders the subsequently deposited copper to interact with the support in order to form $CuAl_2O_4$ so the copper is well dispersed on the surface of the sample.

Adsorption–desorption isotherms are (not presented) of IV type, while the corresponding hysteresis loops are of HH2 type. The H2–type hysteresis of the isotherms should be associated with the presence of pores with narrow necks or narrowings (ink-bottle model) [15] with all samples.

The mesopore distribution curves for all samples are presented in Fig. 1 as well as the same for the initial AlO(OH). In the case of the single metal samples the shape of the curves resembles the curve of the initial AlO(OH). The deposition of copper and cerium does not change the type of the distribution of the metal-oxide phase in the pore space of the initial texture. Nevertheless, well defined distribution maxima are observed. They are shifted in reference to the curve of AlO(OH) ($\overline{Rp} = 2.2\,\text{nm}$) to the large mesopores and this is an evidence for uniform filling of the fine mesopores (without exception of blocked adsorbed complexes in a part of the necks) and the narrowings between the pores. The shapes of the distribution curves of bimetal supported samples are different. Probably in this case dominates the blocking of the constrictions between the pores (respectively the necks of the "ink-bottle" pores). The bimetallic samples possess the most suitable texture for adsorption and catalysis, where narrow pores combined with transport pores such as mesopores are necessary.

Table 1 Chemical composition, specific surface area, total pore volume and phase composition

Sample	Metal content in solution, (mass.%)		Metal content in sample, (mass.%)		S_{BET}, ($m^2\,g^{-1}$)	Vt, ($cm^3\,g^{-1}$)	Phase composition XRD
	Cu	Ce	Cu	Ce			
AlCeCu	8	3.6	7.4	2.10	269	0.43	CuO and CeO_2
AlsCuCe	8	3.6	6.6	0.97	263	0.41	CeO_2, track of $CuAl_2O_4$
AlCuCe	8	3.6	5.5	1.08	260	0.40	CeO_2, track of $CuAl_2O_4$
AlCu	8	–	11	–	240	0.40	CuO, track of $CuAl_2O_4$
AlCe	–	3.6	–	1.05	265	0.42	CeO_2
AL	–	–	–	–	271	0.45	AlO(OH)

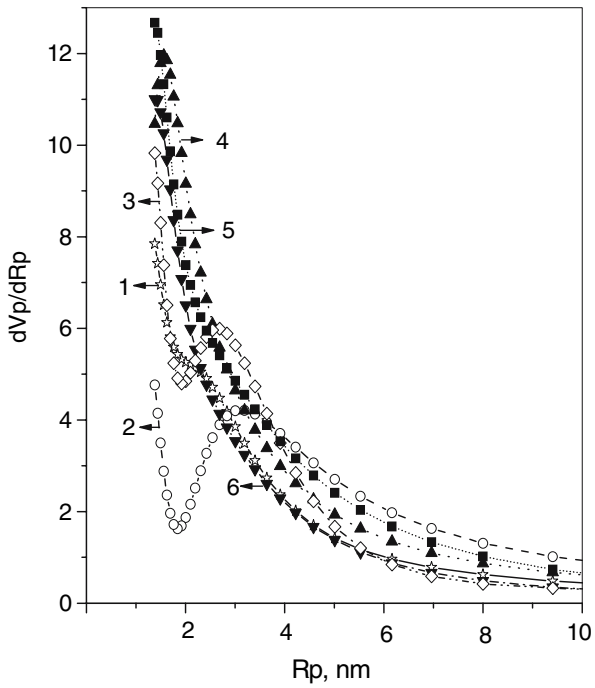

Fig. 1 Pore size distribution curves. AL (1); AlCu (2); AlCe (3); AlCuCe (4); AlCeCu(5); AlsCuCe(6)

3.2 Morphological Analysis

Figure 2 shows the SEM microphotographs of AL, AlCeCu, AlsCuCe and AlCuCe. All samples show both particles with relatively regular (spherical) shapes and larger particles with laminar microstructure. The particle size in AlCeCu and AlsCuCe varies between 0.5 and 2 μm. This probably means that the active phase is supported uniformly. With the sample AlCuCe large regions of a surface oxide film characterized by microcracks are observed.

3.3 XPS Measurements

The X-ray photoelectronic spectra of the investigated samples are presented in Figs. 3 and 4. The Cu $2p_{3/2}$ spectrum in terms of both presence of intense satellite structure and BE value indicates the major part of copper is Cu(II). The positions of the Cu $2p_{3/2}$ at 934.8 eV resembles CuO–Cu(II). The peaks Cu $2p_{3/2}$ at 932.2 eV and 933.1 eV suggest the presence of copper in lower oxidation state as shown in [17]. The main peaks are asymmetric to the side of the lower energies, probably due to the presence of Cu(I) and Cu, as this is more pronounced with the sample AlCeCu. The ratio between the intensities of the main peak to its satellite one for CuO is $I_s/I_m \approx 0.5$. With the sample AlCeCu this ratio is $I_s/I_m \approx 0.4$, and one could conclude that the Cu^+ content in it is larger than in the other samples investigated as in [18]. The surface copper concentration is determined for all samples and for AlCuCe it is 1.2 at.%, for AlsCuCe it is 1.9 at.%, and for AlCeCu—5.1 at.%.

Figure 4 show XPS peaks of the Ce 3d spectral line. The six components (882.3, 888.8, 898.4, 900.8, 907.2 and 916.7 eV) observed in the spectrum can be assigned to Ce(IV) species by comparison with data reported in the literature [19, 20, 21], whereas no signal corresponding to Ce(III) ion is seen in the spectra of AlCuCe and AlsCuCe catalysts. The catalyst AlCeCu shows an inconspicuous peak at 885.8 eV ascribed to the peak of Ce(III) in addition

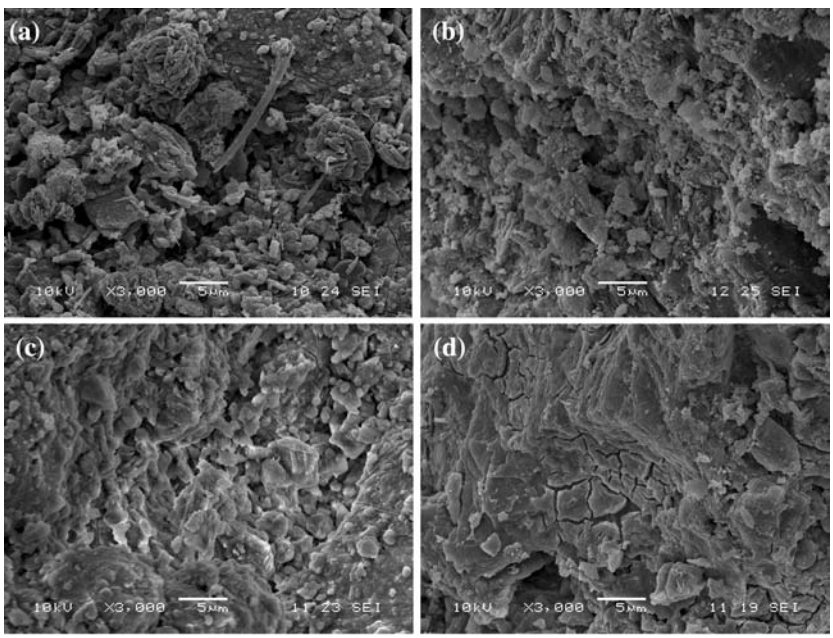

Fig. 2 SEM microphotographs of AL (**a**), AlCeCu (**b**), AlsCuCe (**c**), AlCuCe (**d**)

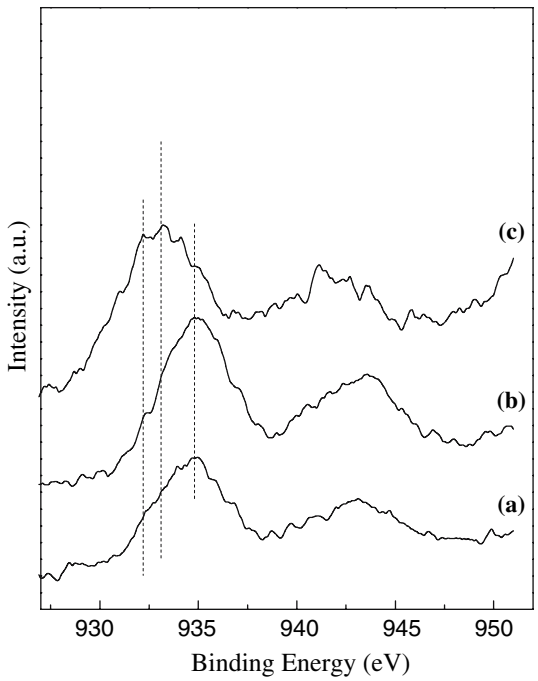

Fig. 3 Cu2p XPS spectra: AlCuCe (**a**); AlsCuCe (**b**); AlCeCu (**c**)

to the peaks of Ce(IV) [22, 11]. The surface cerium concentration is determined to be: AlCuCe—0.8 at.%, AlsCuCe—0.6 at.%, AlCeCu—4.2 at.%.

3.4 Catalytic Studies

Studies on the pure AL support showed its low activity of about 16% for NO and CO at 300 °C. The investigations

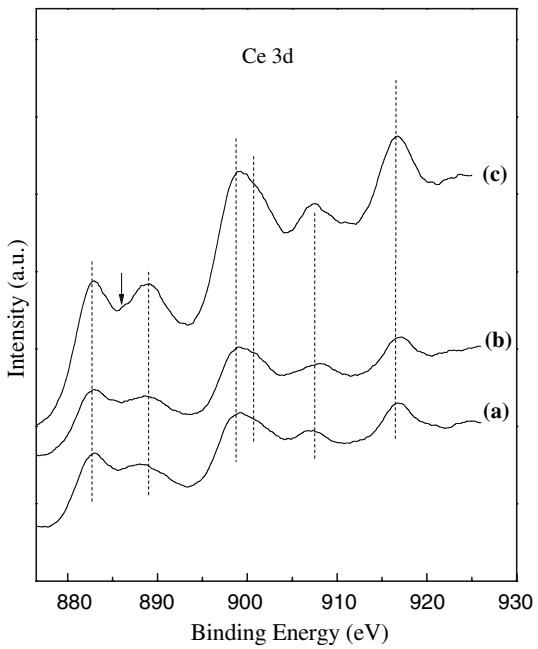

Fig. 4 Ce3d XPS spectra: AlCuCe (**a**); AlsCuCe (**b**); AlCeCu (**c**)

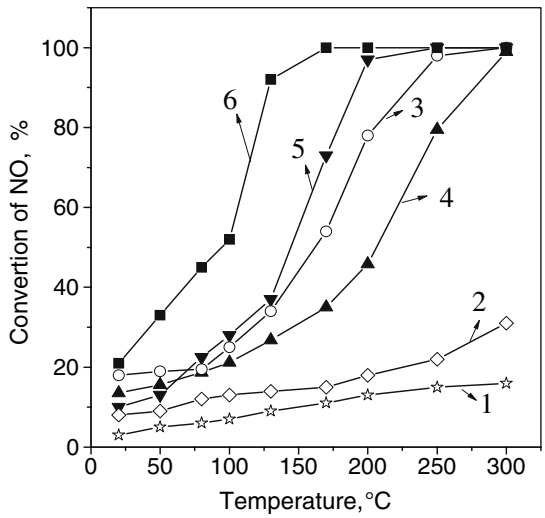

Fig. 5 Temperature dependence of NO conversion degree on samples AL (1); AlCe (2); AlCu (3); AlCuCe (4); AlsCuCe (5) and AlCeCu (6)

have shown that with all samples investigated the reduction of NO with CO proceeds to N_2, i.e. no N_2O is registered in the whole temperature range. Figure 5 and Table 2 illustrate the dependence of the conversion degree of NO on temperature for the bimetal samples with depositions of copper and cerium active phases as well as for the samples with copper or cerium only.

It is obvious that all the samples investigated exhibit a high activity towards the NO reduction with CO, the highest activity belonging to the AlCeCu sample. It is the sample among the bimetal ones which contains the highest copper percentage (Table 1). At 170 °C the conversion of NO with this sample is 98%, while the NO conversions with the AlCuCe and AlCu samples at the same temperature is about 30–50%. The only exception is the sample AlsCuCe where at 170 °C the NO conversion is about 70%.

The results of XRD analysis presented in Table 1 show that only phases of CuO and CeO_2 are observed with the most active sample AlCeCu. All other samples show track of $CuAl_2O_4$. Probably, when the cerium is deposited first as

Table 2 Catalytic activity towards NO in the (NO + CO) reaction at 100 and 170 °C

Sample	η-100 °C (%)	W.10^4 (g m^{-2} h^{-1})	η-170 °C (%)	W.10^4 (g m^{-2} h^{-1})
AlCeCu	52	16.1	98	32.1
AlsCuCe	28	11.1	73	28.6
AlCuCe	21	8.0	34	12.9
AlCu	25	8.6	54	22.9
AlCe	13	5.5	15	6.3
AL	7	2.4	11	3.8

in the case of the sample AlCeCu it covers the surface of the support and doesn't allow the CuO deposited after to interact with the support in order to form $CuAl_2O_4$. Such preparation path ensures good dispersion of CuO on the catalyst surface, as shown in micrographic pictures in Fig. 2. Hence, the way and the sequence of the impregnation during the catalyst preparation strongly affects on the formation of various catalytic sites responsible for the NO conversion at lower temperatures.

Transient response curves for the reagents NO and CO as well for the products N_2 and CO_2 with the sample with the highest activity AlCeCu are shown in Fig. 6. The curves were obtained at temperatures of 50–300 °C under the conditions of a NO + CO + Ar gas mixture. The differences in the curves reveal the rate controlling step of the reaction. The change in the rate-controlling step is associated with a change in the reaction mechanism. Figure 6 shows that at 50 °C the response curves for NO, CO and CO_2 are of a momentous type, i.e. the surface reaction or the reagents adsorption is rate-controlling. The absence of desorption curves at the stop stage indicates the surface reaction at 50 °C to be rate-controlling. At higher temperatures the response curves for NO and CO_2 are already of an overshot type while those for CO preserve their monotonically growing type, this evidencing that the active sites regeneration and the surface reaction are rate-controlling.

The response curves for CO at temperatures of 100 °C and 130 °C show that at the beginning of the transition period there is complete consumption of CO, i.e. carbon monoxide participates not only in the reduction of NO but also in a secondary reduction process on the catalyst surface. The presence of desorption curve for CO at 100 °C in the stop stage indicates the adsorption of CO. A similar picture is observed with AlsCuCe but at higher temperatures above 130 °C.

The results obtained with AlCe show the absence of reduction on the surface, i.e. carbon monoxide participates in NO reduction only and not in a secondary process. With the copper-containing sample AlCu, however, there is a different situation. The results for AlCu resemble, on the whole, the behavior of the bimetal catalyst investigated but the response curve for CO at low temperatures appears later, and at higher temperatures it is of a pronounced monotonically overshot type. This is an indication that, in addition to the reduction of NO, CO is also consumed for reduction of the sample surface. However, this has not been observed with the AlCe sample.

Figure 7 illustrates the TPD spectra of CO obtained at 25–300 °C for all samples. It is evident that with the bimetal catalysts AlCeCu, AlsCuCe, AlCuCe and AlCu there are desorption peaks for CO. The TPD spectra for CO show only one peak with a maximum at 75 °C. This means that CO is adsorbed on the surface of these samples in the same form. With the samples AlCe and AL no peaks for CO are observed in this temperature range. Hence, CO is not adsorbed on the surface of AlCe and AL.

Figure 8 shows the TPD spectra of NO obtained within the range 25–300 °C for all prepared samples. Two distinct NO desorption peaks correspond to each of the samples investigated, the first one having a maximum at 75 °C, the second at 130 °C for AlCeCu and AlsCuCe and with a maximum at 160 °C for AlCuCe, AlCu and AlCe. With the sample AlCeCu third high-temperature peak with a maximum at 260 °C is observed. With the pure support AL, there is a TPD spectrum for NO which has more than two distinct desorption peaks for NO. These peaks represent probably more forms of NO adsorption. One of them is

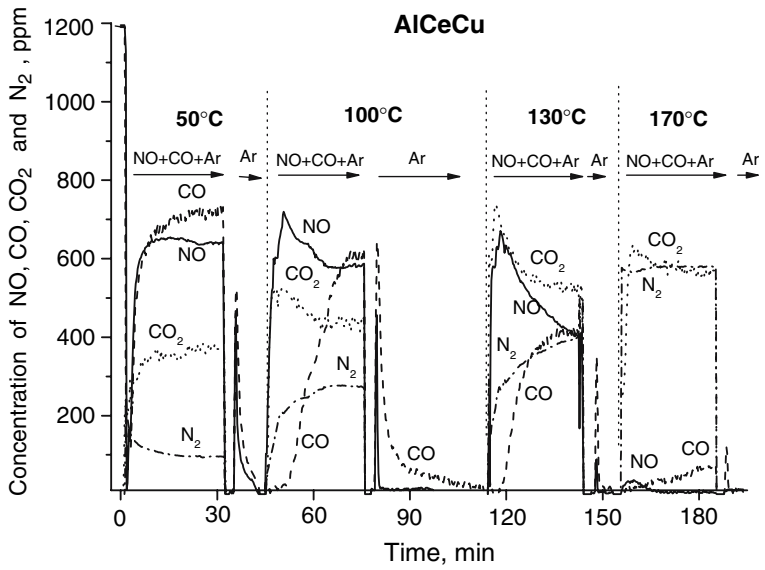

Fig. 6 Transient response curves of NO, CO, CO_2 and N_2 on AlCeCu

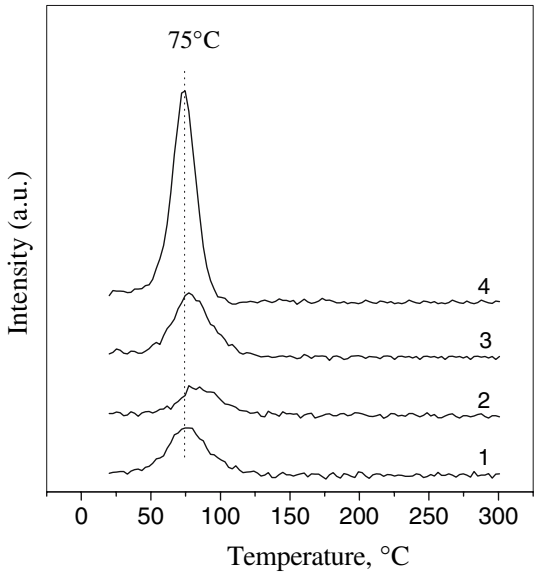

Fig. 7 TPD spectra of CO for AlCu (1); AlCuCe (2); AlsCuCe (3); AlCeCu (4)

more weakly bound and corresponds to the temperature region of the CO form and the others are more strongly bound and are desorbed at higher temperatures. Since adsorption of NO and CO below 80 °C is also observed, this means that at lower temperatures the surface interaction between these two forms is rate-controlling.

The presence of a desorption peak for NO on a pure support indicates that probably the support also participates in the formation of these catalytic active sites on the surface, which are responsible for the reduction of NO. The

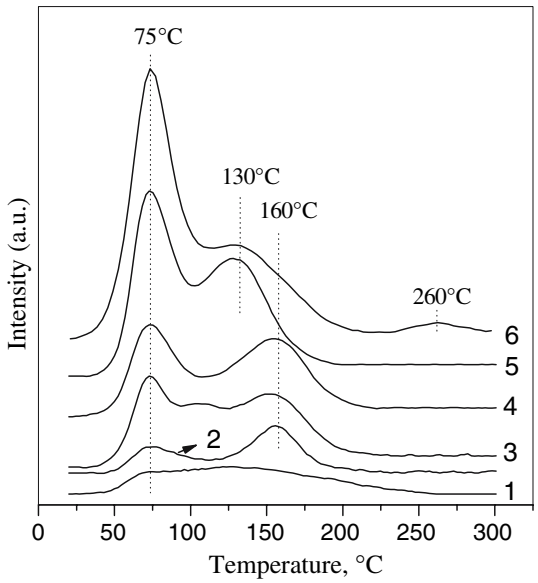

Fig. 8 TPD spectra of NO for AL (1); AlCe (2); AlCu (3); AlCuCe (4); AlsCuCe (5); AlCeCu (6)

catalytic active sites comprise metal ions of the deposited active phase and the support surface. Depending on the supported active phase and on the way of preparation, the temperature and duration of the investigation and the conditions of NO reduction, these catalytic active complexes are reduced or oxidized. The results obtained by the transient response method show that the regeneration of the catalytic active complexes, S^*, is the rate-controlling step and confirm the opinion that with red-ox processes, such as the reduction of NO with CO, the activity depends on the formation, in the catalytic active complexes, of pairs of metal ions in different oxidation states. For copper deposited on active carbon this may be Cu^{2+}–Cu^{+} or Cu^{+}–Cu^{o} [23], for manganese compounds, the couple Mn^{3+}–Mn^{4+} [24], and in cases of mixed unsupported oxides, Cu^{+}–$Mn^{4+} \rightarrow Cu^{2+}$–$Mn^{3+}$. In our case of bimetal catalysts this pair is probably Ce^{4+}–$Cu^{+} \rightarrow Ce^{3+}$–$Cu^{2+}$ which participates in the formation of the catalytic active complexes and the active components in NO + CO reaction were the Cu species (Cu^{2+}, Cu^{+} and Cu^{0}) and the Ce species (Ce^{3+} and Ce^{4+}).

Hence, the following process takes place:

At low temperatures, down to 80°C the following reaction proceeds.

$$CO + S \rightarrow CO_2 + S^* \quad (1)$$

$$S^* + NO + CO \rightarrow CONO(S^*) \quad (2)$$

$$CONO(S^*) \rightarrow CO_2 + 1/2\,N_2 + S \quad (3)$$

At higher temperatures, the reactions take place:

$$CO + S \rightarrow CO_2 + S^* \quad (4)$$

$$S^* + NO \rightarrow NO(S^*) \quad (5)$$

$$NO(S^*) \rightarrow 1/2N_2 + S \quad (6)$$

S—Surface, S^*—Active surface

4 Conclusion

1. The method of preparation leads to the formation of different surface groups on the support and the samples contain different mass% Cu and Ce. The way and the sequence of the preparation strongly affects on the formation of different metal oxide phases and various

catalytic sites responsible for the NO conversion at lower temperatures. However, the addition of cerium to the copper enhances the activity.

2. Two processes: a catalytic one (NO reduction with CO) and a secondary process (interaction of CO with the catalyst surface) occur on the surface of bimetal catalysts and those which active phase is Cu only. The secondary process leads to the formation of a reduced active layer on the surface, which has a stronger affinity to NO. As a result of the secondary process, catalytic active complexes are formed on which NO reduction is easy. Below 80 °C, the rate-controlling step of NO reduction is the surface interaction of the adsorbed reagents. At higher temperatures the reaction proceeds by a red–ox mechanism.
3. Cerium and copper in various oxidation states participate in the formation of catalytic active surface complexes.

References

1. Sheleff M, Otto K, Gandhi H (1968) J Catal 12:361
2. Panayotov D, Khristova M, Mehandjiev D (1987) Appl Catal 34:48
3. Panayotov D, Khristova M, Mehandjiev D (1995) J Catal 156:219
4. Mehandjiev D, Panayotov D, Bliznakov G (1984) Symp "Stic-oxide". Wien, Reports, p 139
5. Panayotov D, Matyshak V, Sklyarov A, Vlasenko A, Mehandjiev D (1986) Appl Catal 24:37
6. Panayotov D, Khristova M, Velikova M (1996) Appl Catal B:Environ 9:107
7. Xiaoyuan J, Liping J, Yingxu Ch, Xiaoming Z (2004) Catal Lett 94:49
8. Xiaoyuan J, Yanrong J, Huang PH, Xiaoming Z (2005) Catal Lett 104:169
9. Park PW, Ledford JS (1998) Catal Lett 50:41
10. Larsson P-O, Andersson A (2000) Appl Catal B:Environ 24:175
11. Zou H, Dong X, Lin W (2006) Appl Surf Sci 253:2893
12. Scofield JH (1976) J Electron Spectrosc Relat Phenom 8:129
13. Kobayashi M (1982) Chem Eng Sci 37:393
14. Jung CR, Han J, Nam SW, Lim TH, Hong SA, Lee HI (2004) Catal Today 93–95:183
15. Rao GR, Sahu HR, Mishra BG (2003) Colloid Surf A:Physico-chem Eng Asp 220:261
16. IUPAC (Phys. Chem. Division) recommendation 1984 (1985) Pure Appl Chem 57:603
17. Zhang Sh-M, Huang W-P, Qiu X-H, Li B-Q, Zheng X-Ch, Wu Sh-H (2002) Catal Lett 80:41
18. Frost DC, Ishitani A, McDowell CA (1972) Mol Phys 24:861
19. Rynkowski J, Farbotko J, Touroude R (2000) Appl Catal A: Gen 203:335
20. Barr TL, Fries CG, Cariati F, Bart JCJ, Giordano N (1983) J Chem Soc, Dalton Trans 9:1825
21. Aboukaïs A, Galtayries A, Abi-Aad E, Courcot D, Grimblot J (1999) Colloid Surf A:Physicochem Eng Asp 154:335
22. Schmieg SJ, Belton DN (1995) Appl Catal B: Environ 6:127
23. Tsoncheva T, Nickolov R, Mehandjiev D (2001) React Kinet Catal Lett 72:389
24. Spassova I, Mehandjiev D (1996) React Kinet Catal Lett 58:57